Noise-based passive ballistic wave seismic monitoring on an active volcano

Tomoya Takano, Florent Brenguier, Michel Campillo, Aline Peltier, Takeshi Nishimura

Geophysical Journal International

Geophys. J. Int. (2020) **220,** 501–507
Advance Access publication 2019 October 18
GJI Seismology

doi: 10.1093/gji/ggz466

Noise-based passive ballistic wave seismic monitoring on an active volcano

Tomoya Takano,[1,2,*] Florent Brenguier,[1] Michel Campillo,[1] Aline Peltier[3] and Takeshi Nishimura[2]

[1]*Institut des Sciences de la Terre, Univ. Grenoble Alpes,* 38058, *France. E-mail: ttakno@eri.u-tokyo.ac.jp*
[2]*Department of Geophysics, Graduate School of Science, Tohoku University,* 980-8578, *Japan*
[3]*Observatoire Volcanologique du Piton de la Fournaise, Institut de Physique du Globe de Paris, Sorbonne Paris Cité, Univ. Paris Diderot, CNRS, La Plaine des Cafres, La Réunion, F-*97418 *Paris, France*

Accepted 2019 October 17. Received 2019 September 27; in original form 2019 May 31

SUMMARY

Monitoring temporal changes of volcanic interiors is important to understand magma, fluid pressurization and transport leading to eruptions. Noise-based passive seismic monitoring using coda wave interferometry is a powerful tool to detect and monitor very slight changes in the mechanical properties of volcanic edifices. However, the complexity of coda waves limits our ability to properly image localized changes in seismic properties within volcanic edifices. In this work, we apply a novel passive ballistic wave seismic monitoring approach to examine the active Piton de la Fournaise volcano (La Réunion island). Using noise correlations between two distant dense seismic arrays, we find a 2.4 per cent velocity increase and −0.6 per cent velocity decrease of Rayleigh waves at frequency bands of 0.5–1 and 1–3 Hz, respectively. We also observe a −2.2 per cent velocity decrease of refracted *P* waves at 550 m depth at the 6–12 Hz band. We interpret the polarity differences of seismic velocity changes at different frequency bands and for different wave types as being due to strain change complexity at depth associated with subtle pressurization of the shallow magma reservoir. Our results show that velocity changes measured using ballistic waves provide complementary information to interpret temporal changes of the seismic properties within volcanic edifices.

Key words: Seismic interferometry; Wave propagation; Body waves; Surface waves.

1 INTRODUCTION

Volcanic eruptions are preceded by increase of pressure in the magma feeding system that leads to the inflation of volcanic edifices. Monitoring the volcano deformation is thus important to understand the functioning of an active magmatic system. Geodetic measurements can detect the inflation of volcanic edifice before eruptions (e.g. Davis 1986; Peltier *et al.* 2005; Genco & Ripepe 2010). However, geodetic measurements are deployed at the ground surface in general, leading to difficulties detecting subtle elastic perturbations within volcano interiors at depth.

On the other hand, seismic waves that travel through the interiors of volcanoes are sensitive to structural changes at depth. Continuous temporal changes in seismic velocity can be estimated by computing the cross-correlation functions of ambient seismic noise (we call hereafter 'noise correlations') (e.g. Sens-Schönfelder & Wegler 2006; Brenguier *et al.* 2008a; Wegler *et al.* 2009). By measuring phase differences of the coda wave part of noise correlations, Hadziioannou *et al.* (2011) have detected temporal changes in the seismic velocity of the order of 0.01 per cent. Noise correlations have been successfully applied to detect seismic velocity changes caused by large earthquakes (e.g. Brenguier *et al.* 2008a; Nakata & Snieder 2011), volcanic activities (e.g. Brenguier *et al.* 2008b; Takano *et al.* 2017) and environmental changes (e.g. Meier *et al.* 2010; Lecocq *et al.* 2017).

Although the multiply scattered waves have a high sensitivity to tiny elastic perturbations by sampling the medium for multiple paths, the spatial sensitivity of the coda waves to velocity changes is complex. The sensitivity of diffuse and multiply scattered waves are high around stations and sources, and the sensitivity around the isochronal scattering shell becomes wider with increasing lapse times (Pacheco & Snieder 2005; Rossetto *et al.* 2011; Kanu & Snieder 2015; Margerin *et al.* 2015; Obermann *et al.* 2016). Seismic velocity changes of coda waves thus make it difficult to properly image localized changes of seismic properties at depth.

* Now at Earthquake Research Institute, University of Tokyo, Bunkyo, Japan

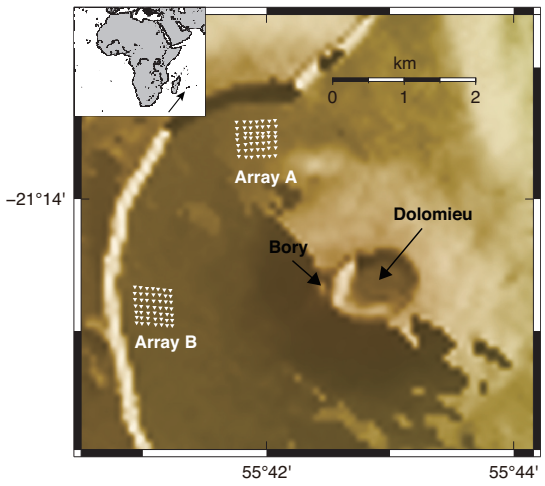

Figure 1. Location of the receivers. The white inverted triangles are geophones. The black arrows point the Dolomieu crater and the Bory crater, respectively. The inset illustrates the location of la Réunion island.

In comparison to coda waves, we can accurately model the travel path of ballistic waves. Brenguier *et al.* (2019) and Mordret *et al.* (2019) propose a novel method for estimating velocity changes of ballistic waves using a dense array and detect velocity changes of refracted *P* waves and direct Rayleigh waves at the Groningen gas field in the Netherlands. The main drawback of using ballistic waves is their strong sensitivity to the bias induced by temporal changes in noise source distribution that can mask physical seismic property changes (Weaver *et al.* 2009; Colombi *et al.* 2014).

In this study, we examine the velocity changes of ballistic waves recovered from noise correlations using two dense arrays on the Piton de la Fournaise volcano. We first calculate noise correlations between two arrays. We then measure temporal changes of apparent seismic velocities of ballistic waves using reconstructed Green's functions. We can estimate temporal changes in velocities from Rayleigh waves at different frequency bands and from refracted *P* waves, thereby we are able to separate the response of the structures at different depths and for different wave types. We finally discuss the origin of the velocity changes during the array observation.

2 DATA

We analyse continuous seismic data recorded by two dense arrays deployed on the Piton de la Fournaise volcano (La Réunion island) (Fig. 1). Piton de la Fournaise is a highly active basaltic volcano. After eruptive activities in 1998–2010, the volcano experienced a quiescence phase of 41 months until a reawakening in 2014 June. A small eruption took place, and 0.4 ± 0.2 Mm^3 products erupted at south–southeast of the summit Dolomieu crater on 2014 June 20–21. The volcano became then quiescent until 2015 February 4–15 when 1.5 ± 0.2 Mm^3 products erupted at the southwest of the summit Bory crater (Peltier *et al.* 2009). During the quiescence phase, three arrays (arrays A, B and C) were deployed at about a same distance from the Dolomieu crater for about 30 d in 2014 July (Brenguier *et al.* 2015). We use the data of array A and array B, each of which is equipped with 49 vertical-component geophones (FarfieldNodal ZLand, the natural frequency of 10 Hz; Hand 2014) with a spacing of about 85 m. Array C is deployed above a complex recent lava flows at south of the crater and not used in the study because noise correlations are unstable (Mao *et al.* 2018).

3 PROCESSINGS

We compute noise correlations of 2401 station pairs between the two arrays. After removing the instrumental response, continuous seismic data are filtered at the frequency band of 0.5–1, 1–3 and 6–12 Hz. We then cut the continuous seismic data into 1 hr segments and apply the spectral whitening and the one-bit normalization to the data in order to reduce effects of source spectra and transient amplitude anomalies (Bensen *et al.* 2007). The ambient noise data at two stations that are selected from arrays A and B are correlated every 1 hr. We then simply stack the noise correlations of which interstation distances are within a 50 m distance bin for the spatial average. We only use the spatial window including more than 50 noise correlations. The noise correlations in the positive and negative lapse times are stacked to enhance the S/N ratio of the Green's functions. Fig. 2 shows the seismic record section of noise correlations as a function of interstation distance. Wave packets with a propagation velocity of about 1 km s^{-1} are seen in the causal and acausal part of noise correlations at 0.5–1 and 1–3 Hz. From the dispersion curve of Rayleigh waves estimated by noise correlations recorded at the Piton de la Fournaise (Brenguier *et al.* 2007), the wave packets propagating with 1 km s^{-1} in the seismic record section denote a direct fundamental mode of Rayleigh waves between the arrays. At the frequency band of 6–12 Hz, we can see the wave packets with a slope of 5 km s^{-1} and an offset of traveltime. Since the 3-D *S*-wave velocity structure on the volcano show a relatively high velocity below the path between two arrays at the shallow depth (Brenguier *et al.* 2007), we assume the extra traveltime is from the near-vertical branch of the path of the refracted wave. The phase of refracted *P* waves has also been identified by a double beamforming analysis between array A and array B by Nakata *et al.* (2016).

We estimate temporal changes in the apparent velocity of direct Rayleigh waves and refracted *P* waves following the method proposed by Brenguier *et al.* (2019). First, we isolate the Rayleigh and refracted *P* waves by applying a 5 per cent cosine tapered window to the noise correlations. Then, we measure the time-shift of noise correlations along interstation distances between different calendar times by the cross-spectrum technique (Poupinet *et al.* 1984). The slope of the time-shifts along distance shows the temporal change of apparent slowness. By multiplying the temporal changes of apparent slowness by a propagation velocity of the ballistic wave, we can estimate the relative temporal change of apparent velocity of the given ballistic wave. The time-shifts are calculated using the time windows of length 6, 3 and 0.6 s at the 0.5–1, 1–3 and 6–12 Hz bands, respectively, which is several times longer than the period of the studied ballistic waves.

We compute seismic velocity changes of ballistic waves from the noise correlations stacked for two different time periods. Mao *et al.* (2018) calculated hourly velocity changes by analysing the coda wave parts of noise correlations at the frequency band of 1–5 Hz within the array A and B and observed velocity decrease of about 0.1 per cent after 2014 July 21. From the hourly velocity changes estimated by Mao *et al.* (2018), we separate the observation period into two periods: 2014 July 4–21 (period 1, before the velocity decrease) and 2014 July 22–28 (period 2, after the velocity decrease). We analyse the noise correlations stacked for period 1

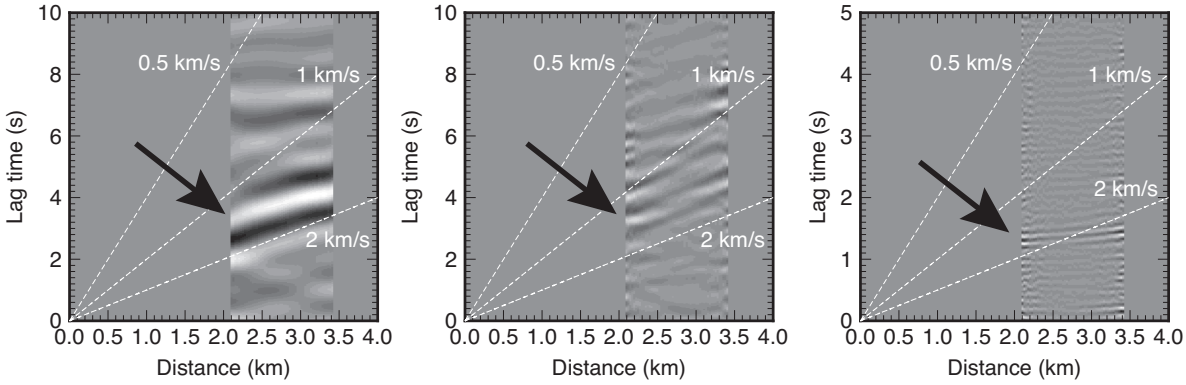

Figure 2. Seismic record sections of noise correlations between receivers of array A and array B at (a) 0.5–1 Hz, (b) 1–3 Hz and (c) 6–12 Hz bands. The white dashed lines show velocity of 0.5, 1 and 2 km s^{-1}. The black arrows point towards possible recovered ballistic waves.

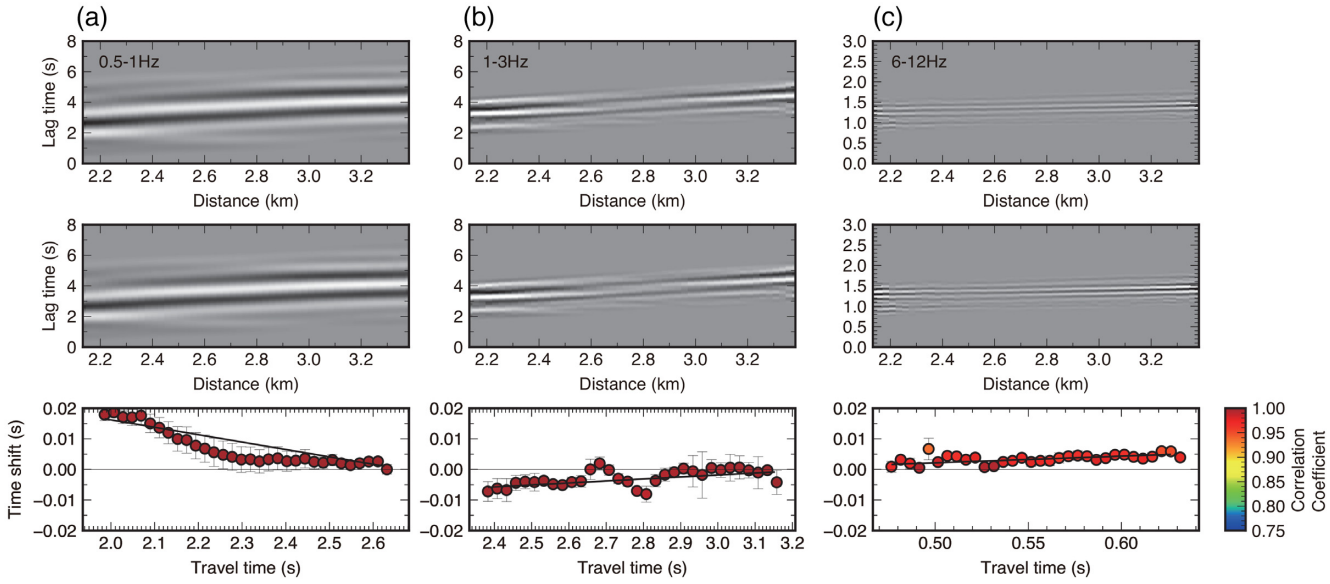

Figure 3. Time-shifts between windowed noise correlations stacked for period 1 and 2 at (a) 0.5–1 Hz, (b) 1–3 Hz and (c) 6–12 Hz bands. (Upper) Windowed noise correlations averaged for the time period from Julian day of 185 to 202. (Middle) Windowed noise correlations averaged for the time period from Julian day of 203 to 208. (Bottom) Time-shifts along interstation distance measured between windowed noise correlations. A colour scale shows the correlation coefficient between a reference and current noise correlations at each distance bin. At 6–12 Hz band, we only use the causal part of noise correlations because of the low SN ratio of Green's function at acausal part.

and period 2 instead of daily velocity changes to enhance the S/N ratio of noise correlations and reduce the apparent time-shifts by temporal changes in the noise source distribution.

4 RESULTS

4.1 Velocity changes of ballistic waves

Fig. 3 illustrates time-shifts between noise correlations stacked for period 1 and period 2. The time-shifts at each frequency band show a clear linear trend along interstation distance, which indicates a clear change in apparent velocity between the two periods. The time offset at a shortest distance for Rayleigh waves is likely associated with the complexity of velocity changes along the propagation path whereas the observed apparent velocity change is localized below the arrays. By multiplying the slope of time-shifts by the apparent velocity of Rayleigh waves at 0.5–1Hz (1.2 km s^{-1}), at 1–3 Hz (1.0 km s^{-1}), and refracted P waves (5 km s^{-1}), we find velocity changes of 2.4 $\pm$ 0.2 per cent, -0.6 ± 0.1 per cent and -2.2 ± 0.2 per cent, respectively. Apparent reference velocity of Rayleigh waves and P waves are obtained from the slope of the wave propagation in the seismic record section.

The increase and decrease of apparent velocity for the Rayleigh waves at the frequency band of 0.5–1 Hz and 1–3 Hz can be attributed to a velocity change at the depth from 0.5 to 3 km and from the ground surface to 0.5 km, respectively, from the depth sensitivity kernel of phase velocity for the fundamental mode Rayleigh waves (see Fig. 5c). The apparent velocity changes for the refracted wave can be directly associated with a real velocity change at a depth at which the wave refracts (Brenguier *et al.* 2019). The depth where the refracted waves propagate is estimated to be 550 m

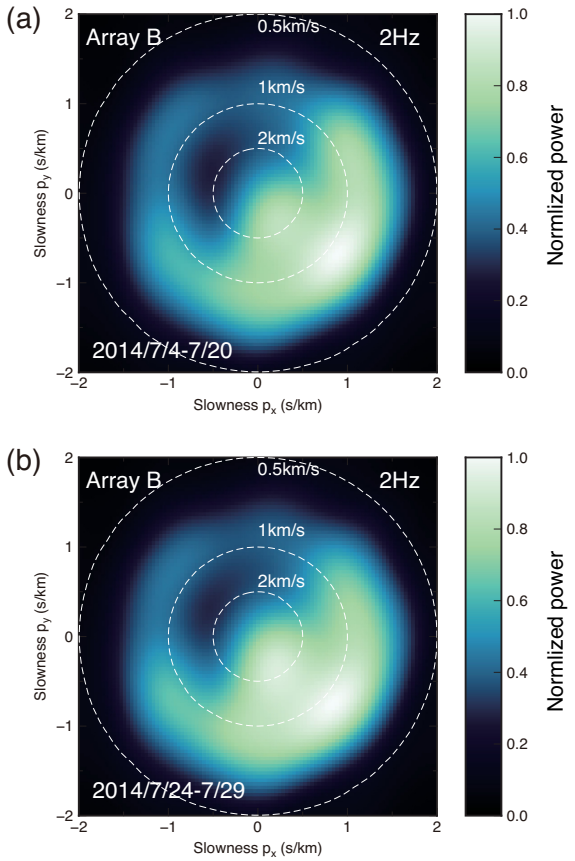

Figure 4. Beamformer outputs of noise data at the frequency of 2 Hz at (a) averaged for the time period from Julian day of 185 to 202 and (b) from Julian day of 203 to 208.

Table 1. Model of noise source intensity for the n-th term.

n	B_n
1	2.0×10^{-3}
2	-1.5×10^{-1}
3	-7.6×10^{-3}
4	5.9×10^{-3}
5	-2.6×10^{-2}
6	-4.0×10^{-2}
7	-6.8×10^{-1}
8	-5.3×10^{-1}

by assuming two velocity layers: The upper layer is 3 km s^{-1} deduced from seismic data (Prôno *et al.* 2009), and the lower layer is 5 km s^{-1} estimated from the noise correlations likely being composed of intrusive solidified basalts known for their high seismic velocities.

5 DISCUSSION

5.1 Effects of noise source distribution variations on observed velocity changes

Passive noise-based seismic monitoring of ballistic waves are highly sensitive to noise source variations compared to that using coda waves (Colombi *et al.* 2014). The errors in apparent arrival times of noise correlations are generated by a non-isotropic distribution of noise source intensity (Weaver *et al.* 2009; Froment *et al.* 2010).

We estimate apparent velocity changes due to temporal changes of a source intensity distribution by applying a beamforming analysis (Rost & Thomas 2002) to the ambient noise data. First, we apply 1-bit normalization to raw seismic noise records and cut data into 20 s long time window. We then calculate cross-spectra for 1d by applying 50 per cent overlapping time windows and estimate beamformer outputs. Since the aperture of the array is larger than the half of maximum wavelength of Rayleigh waves at 0.5–1 Hz band, it is difficult to estimate high-resolution beam power of ambient noise in the frequency range of interest due to the array response function. We here make the assumption that the beam at 2 Hz is representative for ambient noise at the lower frequency bands.

Fig. 4 (a) shows the normalized beam power spectra at the frequency of 2 $\pm$ 0.05 Hz averaged for the period 1 and period 2, respectively, at array B. Noise sources are distributed around the arrays with an apparent velocity of about 1 km s^{-1}, and the high beam power is observed around the azimuth of 130° from the north. Differences of incident azimuth, which is computed by using slowness vectors at the centre-of-mass of beam power, between period 1 and period 2 is 5.2° and 9.2° for array A and array B, respectively.

Apparent arrival time difference between cross-correlations due to variations of a source distribution is formulated by Weaver *et al.* (2009) as follows,

$$\delta t \sim \frac{B''(\varphi_0)}{2t_f \omega_0^2 B(\varphi_0)}, \tag{1}$$

where φ_0 is the azimuth of the path between source and receiver, ω_0 is the angular frequency and t_f is the traveltime. We use the two dimensional equation under the assumption of the noise source distributed on the surface. $B(\theta)$ is the intensity of ambient noise as a function of incident azimuth θ, which is expressed by a Fourier expansion:

$$B(\theta) = B_0 + \sum_{n=1}^{N} B_n \cos(n\theta), \tag{2}$$

where B_0 is the intensity in a case of isotropic source distribution and B_n indicates the intensity of source for the n-th term. We set B_0 to be the averaged beam power at a given apparent velocity. B'' is the second derivative of B with respect to incident azimuth θ. We estimate the intensity terms B by minimizing a misfit function between observed beam power and calculated source intensity with a nonlinear least-squares (Moré 1978) by

$$\sum_{j=0}^{L} \left| B^{obs}(\theta_j) - B^{cal}(\theta_j) \right|^2, \tag{3}$$

where B^{obs} is the observed normalized beamformer output at the apparent velocity of 1 km s^{-1} and frequency of 2 Hz, B^{cal} is the source intensity calculated from eq. (2), and θ_0 is the orientation of the line joining the station and source. We take $\theta_L = \theta_0 + 180°$. Table 1 shows best-fitting model coefficients of source intensity.

The apparent velocity change caused by non-isotropic noise distribution is estimated to be 0.2 per cent between the period 1 and 2, respectively, by dividing the apparent time-shifts by traveltimes. We thus conclude that the observed velocity increase of 2 per cent at the frequency band of 0.5–1 Hz is mostly related to the temporal change of the structure. However, the velocity decrease of −0.6 per cent for the surface wave at the frequency band of 1–3 Hz might be partly biased by temporal changes in the noise source distribution. On the other hand, we cannot directly apply the eq. (2) to apparent time-shifts of body waves because the formulation of Weaver *et al.* (2009) assumes the cylindrical waves in the two dimensions. However, the

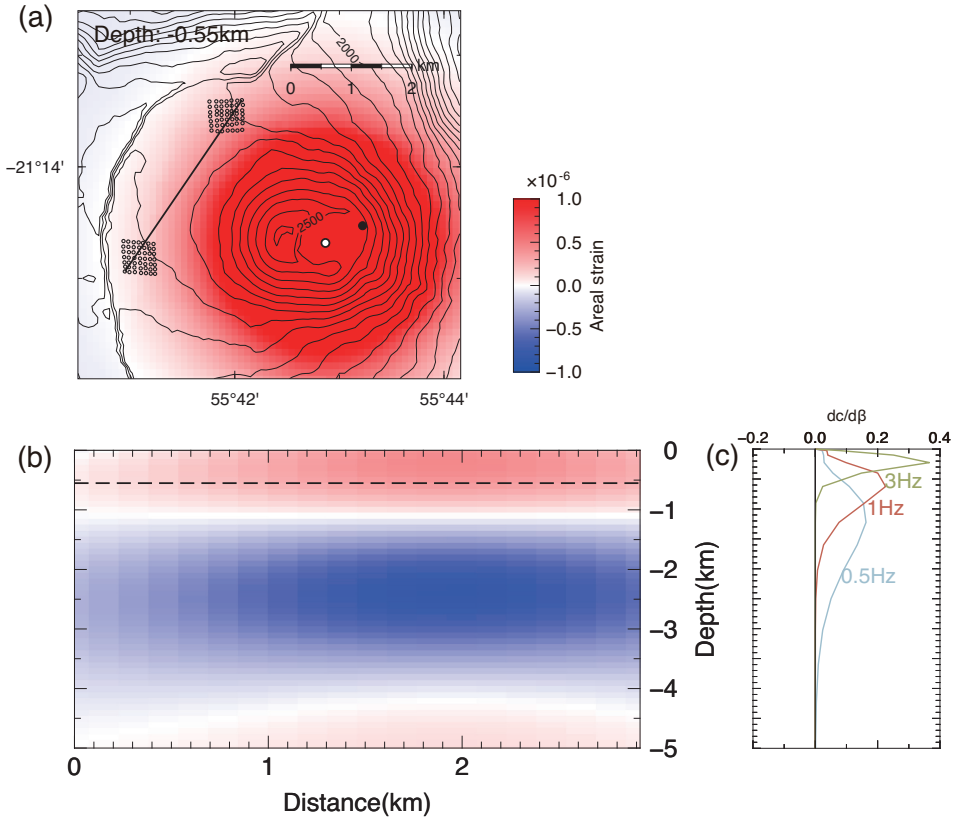

Figure 5. Areal strain by inflation of a pressure source at the depth of 2.3 km. (a) Map view of areal strain for inflation of the 2.3 km depth point source, at the depth of 550 m. The black dot indicates the location of the DERG GPS station. The white dot indicates the location of the pressure source. (b) Cross-section of strain for the thick black line between two arrays shown in (a). The black dashed line shows the depth where *P* waves may refract. (c) Depth sensitivity kernel for relative perturbations in shear wave velocity to phase velocity of the fundamental mode Rayleigh wave at a frequency of 3 Hz (yellow), 1 Hz (red) and 0.5 Hz (blue).

slight variations of source location might not be crucial for apparent time-shifts as long as the phase of body wave is reconstructed from noise correlations because of the appropriate stationary zones for body waves. We thus conclude that the observed velocity changes of the refracted *P* waves are mostly related to temporal changes of the elastic properties in the structure. To accurately evaluate the arrival time-shift by noise source variations considering array geometry, topography and velocity models, we need to calculate time-shifts of cross-correlations by the numerical simulations of wavefields with the noise source sensitivity kernels of traveltimes (Xu *et al.* 2019) and the observed beamformer results.

5.2 Interpretation of velocity changes by volcano deformation

We observe the increase and decrease of Rayleigh wave velocity at the frequency band of 0.5–1 Hz and 1–3 Hz, respectively, and the decrease of refracted *P*-wave velocity at 6–12 Hz band. In this section, we propose a mechanism of the seismic velocity changes based on a magma pressure source in depth.

To interpret the polarity differences of seismic velocity changes for different wave properties, we compute internal areal strain field with inflation of a point pressure source (Mogi 1958) beneath the Dolomieu crater at the depth of 2.3 km, i.e. around the sea level, following the location of the shallowest reservoir evidenced by Peltier *et al.* (2009) (Fig. 5). Since no ground deformation was detected by GPS stations on Piton de la Fournaise during the array observation period, there is no information about a pressure level for the point source at depth. We thus use the value of *P*-wave velocity change to estimate a level of pressure change at the source. From the observed *P*-wave velocity change of −2.2 per cent, the pressure change is estimated to be 3.1×10^4 Pa by using the stress sensitivity of velocity changes 7×10^{-7} Pa^{-1} as inferred from the granular theory (Mavko *et al.* 2009; Takano *et al.* 2017). The volume change is thus estimated to be 2.4×10^5 m^3 by using rigidity of 1.0×10^{10} Pa and Poisson's ratio of 0.25 (Brenguier *et al.* 2008b). The horizontal displacement at the location of GPS station (DERG) is estimated to be 6.2×10^{-4} m by the inflation of the pressure source, which is below the limit of detection of GPS measurements in general. Therefore, the velocity changes of ballistic waves might characterize the magma pressure source which cannot be detected by geodetic measurements.

Fig. 5 shows that areal strain is extensional and compressional above and below the depth of around 1 km, respectively, at the cross-section between two arrays. The depth sensitivity kernel of Rayleigh-wave phase velocities, which is computed by using the velocity structure of Piton de la Fournaise (Mordret *et al.* 2015), shows that Rayleigh waves at the lower frequency band are concentrated at the depth from 0.5 to 2.5 km, while those at the frequency of higher than 1 Hz are concentrated at the depth from the ground surface to 0.5 km (see Fig. 5c). The Rayleigh waves at the frequency band of 0.5–1 Hz thus propagate in the region of compressional strain and could thus explain the velocity increase, while those at the frequency band of 1–3 Hz propagate at the depth where we observe

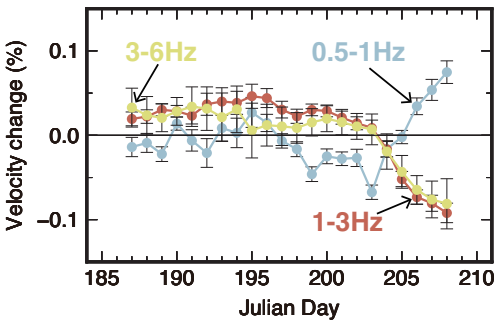

Figure 6. Coda-based daily seismic velocity changes at the frequency band of 0.5–1 Hz (blue), 1–3 Hz (red) and 3–6 Hz (yellow).

extensional strain. On the other hand, refracted *P*-waves propagate at depth of 550 m where we observe extensional strain and could thus explain the velocity decrease.

5.3 Daily velocity changes of coda waves

We estimate seismic velocity changes by using the coda part of noise correlations because coda waves allow us to mitigate the influence of noise source distribution. We analyse the negative and positive lapse times ranging from 10 to 70 s, from 10 to 40 s, and from 5 to 15 s at the frequency band of 0.5–1, 1–3 and 3–6 Hz, respectively. Daily seismic velocity changes are estimated by applying a moving window of the cross-spectrum method to noise correlations. We obtain daily noise correlations by stacking noise correlations for 5 d long with a 1 d moving window and reference noise correlations by stacking over the observation period. We estimate daily seismic velocity changes by fitting a weighted linear regression line to the time-shifts averaged for all station pairs (Fig. 6). Seismic velocity increases up to 0.08 per cent after the Julian day of 204 (2014 July 24) at the frequency band of 0.5–1 Hz, while seismic velocity decreases down to −0.1 per cent at the frequency bands of 1–3 Hz and 3–6 Hz after the Julian day of 204. The magnitudes of seismic velocity changes at the frequency of higher than 1 Hz are consistent with the velocity changes estimated by using noise correlations within the same arrays at Piton de la Fournaise (Mao *et al.* 2018). However, note that magnitudes of velocity changes are one order smaller than those estimated using the ballistic waves. In comparison with ballistic waves, coda waves might sample both extensional and compressional strains because of spatial sensitivity kernel of coda wave and mix of different modes.

6 CONCLUSION

We have examined the seismic velocity changes of ballistic waves by using dense arrays at Piton de la Fournaise volcano. Seismic velocity changes of Rayleigh waves at the frequency band of 0.5–1 Hz and 1–3 Hz are estimated to be 2.4 ± 0.2 per cent and −0.6 ± 0.1 per cent, respectively, and velocity changes of refracted *P* waves at 550 m depth at the frequency band 6–12 Hz are estimated to be −2.2 ± 0.2 per cent. Different polarities of velocity changes of Rayleigh waves and refracted *P* waves may be caused by inflation of a magma pressure source (i.e. the shallowest magma reservoir) at 2.3 km depth. The volume change of the pressure source as inferred from the velocity change of *P* wave is below the detectability threshold of GPS measurements, which indicates that velocity changes of ballistic waves are able to characterize a magma pressure source which has not been detected by geodetic measurements. Velocity changes of ballistic waves could provide complementary information to understand the temporal changes in the seismic properties within volcanic edifices.

ACKNOWLEDGEMENTS

We thank a VolcArray project for providing us the continuous seismic data. VolcArray is a joint project between ISTerre, Observatoire Volcanologique du Piton de la Fournaise (OVPF), Institut de Physique du Globe de Paris (IPGP) and Parc National de la Réunion. The data are available without restrictions from the RESIF and EIDA data centres under the FDSN network code XP (doi:10.15778/RESIF.XP2014). We acknowledge support from the French ANR grant T-ERC 2018 (FaultProbe), the European Research Council under grants no. 742335, F-IMAGE and no. 817803 FAULTSCAN, and the European Union's Horizon 2020 research and innovation program under grant agreement No. 776622 (PACIFIC). Tomoya Takano is grateful for support from the Japan Society for the Promotion of Science (JSPS) and the International Joint Graduate Program in Earth and Environmental Sciences (GPEES). This is IPGP contribution number 4074. We acknowledge P. Boué, H. Nakahara and H. Pedersen for useful discussions. We thank Dr Andrea Morelli, Dr Kees Wapenaar, and Dr Laura Ermert for their comments which significantly improved the manuscript.

REFERENCES

Bensen, G., Ritzwoller, M., Barmin, M., Levshin, A., Lin, F., Moschetti, M., Shapiro, N. & Yang, Y., 2007. Processing seismic ambient noise data to obtain reliable broad-band surface wave dispersion measurements, *Geophys. J. Int.,* **169**(3), 1239–1260.

Brenguier, F., Shapiro, N.M., Campillo, M., Nercessian, A. & Ferrazzini, V., 2007. 3-D surface wave tomography of the piton de la fournaise volcano using seismic noise correlations, *Geophys. Res. Lett.,* **34**(2), doi:10.1029/2006GL028586.

Brenguier, F., Campillo, M., Hadziioannou, C., Shapiro, N., Nadeau, R.M. & Larose, E., 2008a. Postseismic relaxation along the San Andreas fault at Parkfield from continuous seismological observations, *Science,* **321**(5895), 1478–1481.

Brenguier, F., Shapiro, N.M., Campillo, M., Ferrazzini, V., Duputel, Z., Coutant, O. & Nercessian, A., 2008b. Towards forecasting volcanic eruptions using seismic noise, *Nat. Geosci.,* **1**(2), 126–130.

Brenguier, F. *et al.*, 2015. Toward 4d noise-based seismic probing of volcanoes: perspectives from a large-n experiment on piton de la fournaise volcano, *Seismol. Res. Lett.,* **87**(1), 15–25.

Brenguier, F. *et al.*, 2019. Noise-based ballistic body-wave passive seismic monitoring - Part1: Body-waves, *Geophys. J. Int.,* in press.

Colombi, A., Chaput, J., Brenguier, F., Hillers, G., Roux, P. & Campillo, M., 2014. On the temporal stability of the coda of ambient noise correlations, *C. R. Geosci.,* **346**(11), 307–316.

Davis, P.M., 1986. Surface deformation due to inflation of an arbitrarily oriented triaxial ellipsoidal cavity in an elastic half-space, with reference to Kilauea volcano, Hawaii, *J. geophys. Res.,* **91**(B7), 7429–7438.

Froment, B., Campillo, M., Roux, P., Gouédard, P., Verdel, A. & Weaver, R.L., 2010. Estimation of the effect of non-isotropically distributed energy on the apparent arrival time in correlations, *Geophysics,* **75**(5), SA85–SA93.

Genco, R. & Ripepe, M., 2010. Inflation-deflation cycles revealed by tilt and seismic records at stromboli volcano, *Geophys. Res. Lett.,* **37**(12), doi:10.1029/2010GL042925.

Hadziioannou, C., Larose, E., Baig, A., Roux, P. & Campillo, M., 2011. Improving temporal resolution in ambient noise monitoring of seismic wave speed, *J. geophys. Res.,* **116**(B7), doi:10.1029/2011JB008200.

Hand, E., 2014. A boom in boomless seismology, *Science ,* **345,** 720–721.

Kanu, C. & Snieder, R., 2015. Time-lapse imaging of a localized weak change with multiply scattered waves using numerical-based sensitivity kernel, *J. geophys. Res.,* **120**(8), 5595–5605.

Lecocq, T., Longuevergne, L., Pedersen, H.A., Brenguier, F. & Stammler, K., 2017. Monitoring ground water storage at mesoscale using seismic noise: 30 years of continuous observation and thermo-elastic and hydrological modeling, *Sci. Rep.,* **7**(1), 14241.

Mao, S., Campillo, M., Hilst, R.D., Brenguier, F., Stehly, L. & Hillers, G., 2018. High temporal resolution monitoring of small variations in crustal strain by dense seismic arrays, *Geophys. Res. Lett.,* **46,** 128–137.

Margerin, L., Planès, T., Mayor, J. & Calvet, M., 2015. Sensitivity kernels for coda-wave interferometry and scattering tomography: theory and numerical evaluation in two-dimensional anisotropically scattering media, *Geophys. J. Int.,* **204**(1), 650–666.

Mavko, G., Mukerji, T. & Dvorkin, J., 2009. *The Rock Physics Handbook: Tools for Seismic Analysis of Porous Media,* Cambridge University Press.

Meier, U., Shapiro, N.M. & Brenguier, F., 2010. Detecting seasonal variations in seismic velocities within Los Angeles basin from correlations of ambient seismic noise, *Geophys. J. Int.,* **181**(2), 985–996.

Mogi, K., 1958. Relations between the eruptions of various volcanoes and the deformations of the ground surfaces around them, *Bull. Earth. Res. Inst.,* **36,** 99–134.

Mordret, A., Rivet, D., Landès, M. & Shapiro, N.M., 2015. Three-dimensional shear velocity anisotropic model of piton de la fournaise volcano (la réunion island) from ambient seismic noise, *J. geophys. Res.,* **120**(1), 406–427.

Mordret, A. *et al.*, 2019. Noise-based ballistic waves passive seismic monitoring - part 2: Surface waves, *Geophys. J. Int.,* in press.

Moré, J.J., 1978. The Levenberg-Marquardt algorithm: implementation and theory, in *Numerical Analysis,* pp. 105–116, ed. Watson, G.A. , Springer.

Nakata, N. & Snieder, R., 2011. Near-surface weakening in Japan after the 2011 Tohoku-Oki earthquake, *Geophys. Res. Lett.,* **38**(17), doi:10.1029/2011GL048800.

Nakata, N., Boué, P., Brenguier, F., Roux, P., Ferrazzini, V. & Campillo, M., 2016. Body and surface wave reconstruction from seismic noise correlations between arrays at piton de la fournaise volcano, *Geophys. Res. Lett.,* **43**(3), 1047–1054.

Obermann, A., Planès, T., Hadziioannou, C. & Campillo, M., 2016. Lapse-time-dependent coda-wave depth sensitivity to local velocity perturbations in 3-d heterogeneous elastic media, *Geophys. J. Int.,* **207**(1), 59–66.

Pacheco, C. & Snieder, R., 2005. Time-lapse travel time change of multiply scattered acoustic waves, *J. acoust. Soc. Am.,* **118**(3), 1300–1310.

Peltier, A., Ferrazzini, V., Staudacher, T. & Bachelery, P., 2005. Imaging the dynamics of dyke propagation prior to the 2000–2003 flank eruptions at piton de la fournaise, reunion island, *Geophys. Res. Lett.,* **32**(22), doi:10.1029/2005GL023720.

Peltier, A., Bachèlery, P. & Staudacher, T., 2009. Magma transport and storage at piton de la fournaise (la réunion) between 1972 and 2007: A review of geophysical and geochemical data, *J. Volcanol. Geotherm. Res.,* **184**(1-2), 93–108.

Poupinet, G., Ellsworth, W. & Frechet, J., 1984. Monitoring velocity variations in the crust using earthquake doublets: An application to the Calaveras fault, California, *J. geophys. Res.,* **89**(B7), 5719–5731.

Prôno, E., Battaglia, J., Monteiller, V., Got, J.-L. & Ferrazzini, V., 2009. P-wave velocity structure of piton de la fournaise volcano deduced from seismic data recorded between 1996 and 1999, *J. Volcanol. Geotherm. Res.,* **184**(1-2), 49–62.

Rossetto, V., Margerin, L., Planes, T. & Larose, E., 2011. Locating a weak change using diffuse waves: Theoretical approach and inversion procedure, *J. Appl. Phys.,* **109**(3), 034903.

Rost, S. & Thomas, C., 2002. Array seismology: Methods and applications, *Rev. geophys.,* **40** (3), 2–1-2-27.

Sens-Schönfelder, C. & Wegler, U., 2006. Passive image interferometry and seasonal variations of seismic velocities at Merapi volcano, Indonesia, *Geophys. Res. Lett.,* **33**(21), L21302.

Takano, T., Nishimura, T. & Nakahara, H., 2017. Seismic velocity changes concentrated at the shallow structure as inferred from correlation analyses of ambient noise during volcano deformation at Izu-Oshima, Japan, *J. geophys. Res.,* **122**(8), 6721–6736.

Weaver, R., Froment, B. & Campillo, M., 2009. On the correlation of non-isotropically distributed ballistic scalar diffuse waves, *J. acoust. Soc. Am.,* **126**(4), 1817–1826.

Wegler, U., Nakahara, H., Sens-Schönfelder, C., Korn, M. & Shiomi, K., 2009. Sudden drop of seismic velocity after the 2004 mw 6.6 mid-Niigata earthquake, Japan, observed with passive image interferometry, *J. geophys. Res.,* **114**(B6), B06305.

Xu, Z., Mikesell, T.D., Gribler, G. & Mordret, A., 2019. Rayleigh-wave multicomponent cross-correlation-based source strength distribution inversion. part 1: Theory and numerical examples, *Geophys. J. Int.,* **218**(3), 1761–1780.